December 2009 Volume 5 Issue 4

Trade Science Inc.

Materials Science

An Indian Journal

Full Paper

MSAIJ, 5(4), 2009 [387-395]

# Processing, structural and microstructural properties of zirconium doped 212-Bi-Sr-vanadate ferroelectrics ceramics

**M.Morsy Abou Sekkina[1], M.Khaled Elsabawy[2,*], A.Mohamed Asker[1]**

[1]Materials Science Unit, Chemistry Department, Faculty of Science, Tanta University-31725, (EGYPT)

[2]Materials Science Unit, Faculty of Science, Taif University- Taif City, Alhawyah-888, (SAUDI ARABIA)

E-mail : ksabawy@Yahoo.com

*Received: 18th October, 2009 ; Accepted: 28th October, 2009*

## ABSTRACT

The present samples having the general formula $Bi_2SrV_{2-x}Zr_xO_9$, where (x=0.05, 0.1, 0.2, 0.3, 0.6) were carefully synthesized and processed by using solid state reaction route and sintering temperature at 850°C for 10 hrs. TGA and DTA thermal analyses were carried out on the green mixture to identify the best thermal treatment for processing of Bi-Sr-V-O system. XRD-analysis of the prepared samples proved that Zr-dopant can substitute successfully until x=0.6 mole on the Bi-layered perovskite crystal structure. SE-microscopy indicated that the average grain size was found to be in between 1.5 and 1.9μm. Zr - dopings have slight effects on both ESR-signals and conduction mechanism of Zr-doped Bi-Sr-VO regime.



## KEYWORDS

Bi-Vanadates;
Zr-dopant;
Perovskite;
Ceramic;
X- ray;
SEM;
ESR;
IR.

## INTRODUCTION

The bismuth-oxide layered perovskite materials such as Bi-Sr-V-O have attracted increasing attention in the research community because they are fatigue-free and lead free[1-3].

The wide spread application and commercialization of bismuth- layered perovskite ferroelectrics have been limited by drawbacks, their rather high processing temperature and their relatively low remanent polarization[4,5]. Recently, efforts have been made to enhance the properties of layered perovskite ferroelectrics by addition or substitution of alternative cations[6-8].

It's now well established that the variation of oxygen content and distribution of oxygen atoms on the lattice site strongly influences the physical and structural properties (e.g. electrical conductivity) at high-temperature. Superconductors and many other metallic oxides[9].

The discovery of high temperature superconductors has attracted much attention for their technological application such as superconducting quantum interference devices (SQUID), The high Tc ceramic superconductor, the Bi-based system has been studied because of its high critical temperature especially with the partial substitution of Pb in Bi and Sr sites since it promotes the stabilization of 2223 phase when grown from 2212 phase[10,11].

Aurivillius published a series of papers[12-14] explaining the discovery of mixed metal oxides having bismuth layer alternating with perovskite structure layers, because of their ionic structural framework, Aurivillius

phases exhibit great flexibility with respect to metal cation substitution. Therefore, these phases have high potential for systematic control of their properties[15].

There are different studies showing the chemical substitution such as Pb doping on Bi-O layers that can be used to improve conduction in the blocking layers and so to a large decrease in the resistivity anisotropy. The reduced anisotropy leads to improvement of the critical current in the heavy Pb-doped[16-18].

It's shown that the Sn doping in Bi-system superconductors does not change the Tc significantly[19,20]. Shrivastava et al.[21] found that the incorporation of La cations into A sites up to 50% continuously decreased the Curie temperature in SBN ferroelectric ceramics.

Das et al.[22] reported the improved remanent polarization of SBN and $SrBi_2Ta_2O_9$ this films, when a small amount of Ca cations were incorporated into A sites: Bismuth layered perovskite materials have high fatigue resistance[23] and therefore have attracted an increasing attention for non-volatile random access memory (NVRAM) application[24].

The crystal structure and chemical composition of these layered perovskites were systematically studied[25] with the general formula of $(Bi_2O_2)^{2+}(Am^{-1}BmO^{3}m^{+1})^{3-}$, consisting of m-perovskite unites sandwiched between bismuth oxide layers called the family of bismuth layered structured ferroelectrics[26], where A and B two types of cations that enter the perovskite unite A is $Bi^{3+}$, $Ba^{2+}$, $Sr^{2+}$, and B is $Ti^{4+}$, $Ta^{5+}$, and m=1-6 layered perovskite strontium tantalite is a member of bismuth layer- structured ferroelectrics.

The crystal structure of Sr $Bi_2Ta_2O_9$ comprises pseudo- perovskite blocks $(SrTa_2O_7)^{2-}$ that are sandwiched between $(Bi_2O_2)^{2+}$ layers. Sr occupies the A site of the perovskite block and Ta occupies the B-site[27].

The essential goal of the present article is to investigate wide range of Zr-dopings on- vanadium sites of 212 Bi-Sr-V-O regime on;

(a) Structural & microstructure properties.
(b) Thermal and processing temperature.
(c) Spectroscopic properties (IR, ESR).
(d) Conduction behaviour of 212-Bi-Sr-V-O, system.

## EXPERIMENTAL

The pure $Bi_2SrV_2O_9$ and doped samples with the general formula $Bi_2SrV_{2-x}Zr_xO_9$, where x=0.05, 0.1, 0.2, 0.3, 0.6 mole were prepared by conventional solid state reaction route and sintering procedure using the appropriate amounts of $Bi_2(CO_3)_3$, $SrCO_3$, $(NH_4)_2VO_3$ and $ZrO_2$ (each purity>99%). The mixture was ground in an agate mortar for one hour. Then the finely ground powder was subject to firing at 800°C for 10 hours, reground and finally pressed into pellets with thickness 0.2cm, diameter 1.2cm and Sintered at 850°C for 10hours. Then the furnace is cooled slowly down to room temperature. Finally the materials are kept in vacuum desiccator over silica gel dryer.

### Structural measurements

### X-Ray diffraction (XRD)

The X-ray diffraction measurements (XRD) were carried out at room temperature on the fine ground $Bi_2SrV_2O_9$ and $Bi_2SrV_{2-x}Zr_xO_9$ systems in the range ($2\theta$=10-70°) using Cu-K$\alpha$ radiation source and a computerized [Bruker Axs-D8 advance] X-ray diffractometer with two theta scan technique.

### Scanning electron-microscope

Scanning electron microscope (SEM) measurements were carried out using small pieces of prepared samples on different sectors to be the actual molar ratios by using "TXA-840, JEOL-Japan" attached to XL30 apparatus with EDX unit, accelerant voltage 30kv, magnification 10x up to 500.000x and resolution 3nm. The samples were coated with gold.

### Conductivity measurements

The DC-electrical conductivity of the samples was measured using the two terminals DC-method. The pellets were inserted between spring loaded copper electrodes, A KEITHLEY 175 multimeter (ASA) was employed from room temperature up to 500K. The temperature was measured by a calibrated chromel-alumel thermocouple placed firmly at the sample. Measurements were conducted in such a way that at each temperature, sufficient time was allowed to attain thermal equilibration.

### Thermal analyses measurements

The thermogravimetric analysis (TGA) and the differential thermal analysis (DTA) measurements were carried out on the green mixtures (starting powders) of

the prepared samples using a computerized Shimadzu c Japan TGA/DTA analyzer and $Al_2O_3$ as a reference for DTA measurements.

### Solid infrared absorption spectral measurements

The IR absorption spectra of the prepared samples were recorded using "Nexus 670 FT IR spectrometer in the range 500-2500cm$^{-1}$ using pure KBr matrix".

### Electron paramagnetic resonance measurements

The electron spin resonance spectra (ESR) were recorded at room temperature for the prepared samples using at x-band frequencies on a "Bruker-ELEXSYS E 500 Germany" spectrometer at the National Research Center, Egypt.

## RESULTS AND DISCUSSION

### Phase identification

### X-Ray diffraction

The X-ray diffraction patterns of pure and Zr-doped samples with the general formula $Bi_2SrV_{2-x}Zr_xO_9$, where x=0.05, 0.1, 0.2, 0.3, 0.6 mole are shown in Figure ($1_{a-f}$).

Analysis of the corresponding 2θ values and the interplanar spacing d (A°) by using computerized program proved that the compound is mainly belongs to distorted perovskite type with hexagonal crystal form, that expressed by assigned peaks in major .

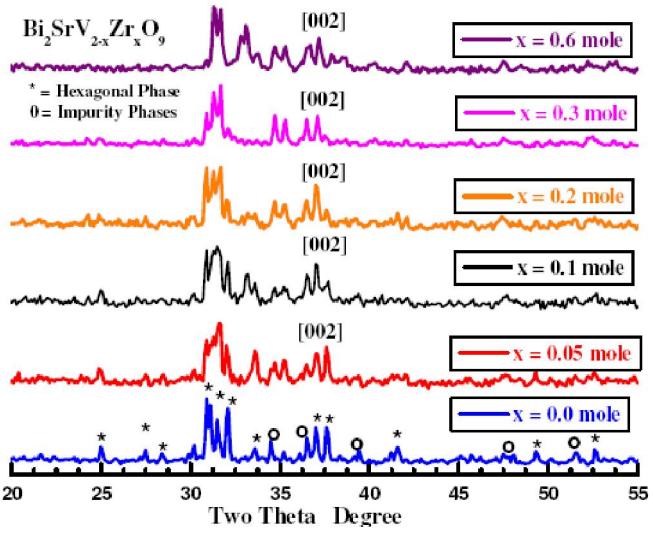


**Figure ($1_{a-f}$) : XRD patterns recorded for (a) pure $Bi_2SrV_2O_9$ and Zr-doped samples (b):$Bi_2SrV_{1.95}Zr_{0.05}O_9$, (c):$Bi_2SrV_{1.9}Zr_{0.1}O_9$, (d): $Bi_2SrV_{1.8}Zr_{0.2}O_9$, (e):$Bi_2SrV_{1.7}Zr_{0.3}O_9$, (f):$Bi_2SrV_{1.4}Zr_{0.6}O_9$**

The unite cell dimensions were calculated using parameters of the most intense X-ray reflection peaks and found to be a= b=5.7804 A° and c=7.104A° for the pure 212Bi-Sr-V-O. Single phase of the layered perovskite structure appeared when Zr is up to or equal 0.05[28]. The substitution of $Zr^{4+}$ for $V^{5+}$ in BSV would induce A-site cation vacancies in perovskite layers, which leads to an increase of internal stress for the shrinkage of unite cell volume[29]. The increasing of Zr ions in the crystal lattice of BSV will result in strong stress, which will expel other Zr -ions from the crystal lattice of BSV.

The layered perovskite structure would be more restrictive since $(Bi_2O_2)^{2+}$ interlayeres impose a great constraint for structural relaxation. Such a structural constraint induced from $(Bi_2O_2)^{2+}$ interlayeres may well explain the lack of an appreciable decrease in lattice parameters with an increased amount of vanadium dopping[30].

From Figure (2) It is clear that *c-axis* increases as result of substitution Zr- dopant on the bases of ionic radius it is expected that *c-axis* increases as $Zr^{4+}$ doping ratio increases. Furthermore, $Zr^{4+}$ is lower in charge than $V^{5+}$ and as a result it is expected to decrease stress inside lattice and consequently the shrinkage factor of lattice will be increased.

From Figure ($1_{a-f}$), It is clear that the Zr-substitutions are successful in the most of investigated range even at high concentration x=0.6 mole since there is no evidence noticeable at X-ray diffractogram referring to Zr-impurity phase. This confirms that Zr-dopant can substitute in the V-sites successfully in the whole investigated range.

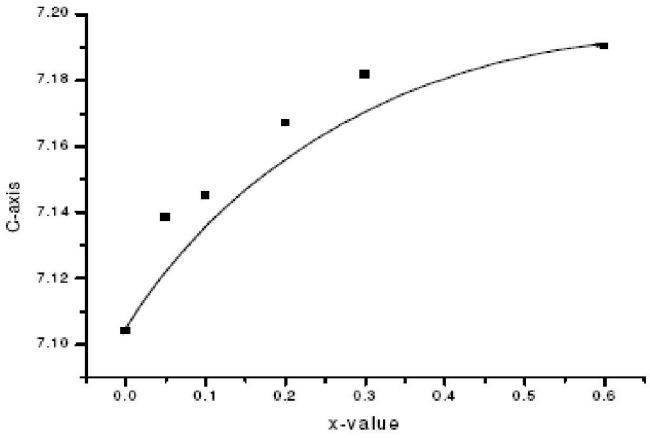


**Figure (2) : Variation of *c-axis* as a function of Zr-content**

Full Paper

## Microstructural properties (SEM)

Figure ($3_{a-c-e}$) shows the scanning electron micrographs recorded for pure 212-Bi-Sr-V-O system and Zr-doped having the formula $Bi_2SrV_{2-x}Zr_xO_9$, where x=0.1, 0.3 mole.

The average grain size of pure and Zr-doped 212-Bi-Sr-V-O system were calculated carefully and found to be in between 1.5-1.9μm which is totally matched with those reported in the literatures[31-32].

Figure ($3_{a-c-e}$) for pure Bi-212 shows that the high content of bismuth results in attraction for the grain with each others and porous appeared between the grains due to bismuth evaporation.

For sample with Zr-doping (0.1,0.3), the Zr ions connect to grain with other, the increasing of Zr concentration leads to increase of grain size from 1.58μm in pure Bi-212 to 1.901μm and 1.981μm for x=0.1 and 0.3 respectively (Figure $2_{a-c-e}$).

From Figure ($3_{a-c-e}$) one can notify that there is no sharp differences in the grey colouration that reflects homogeneity and the quality of processing of 212-Bi-

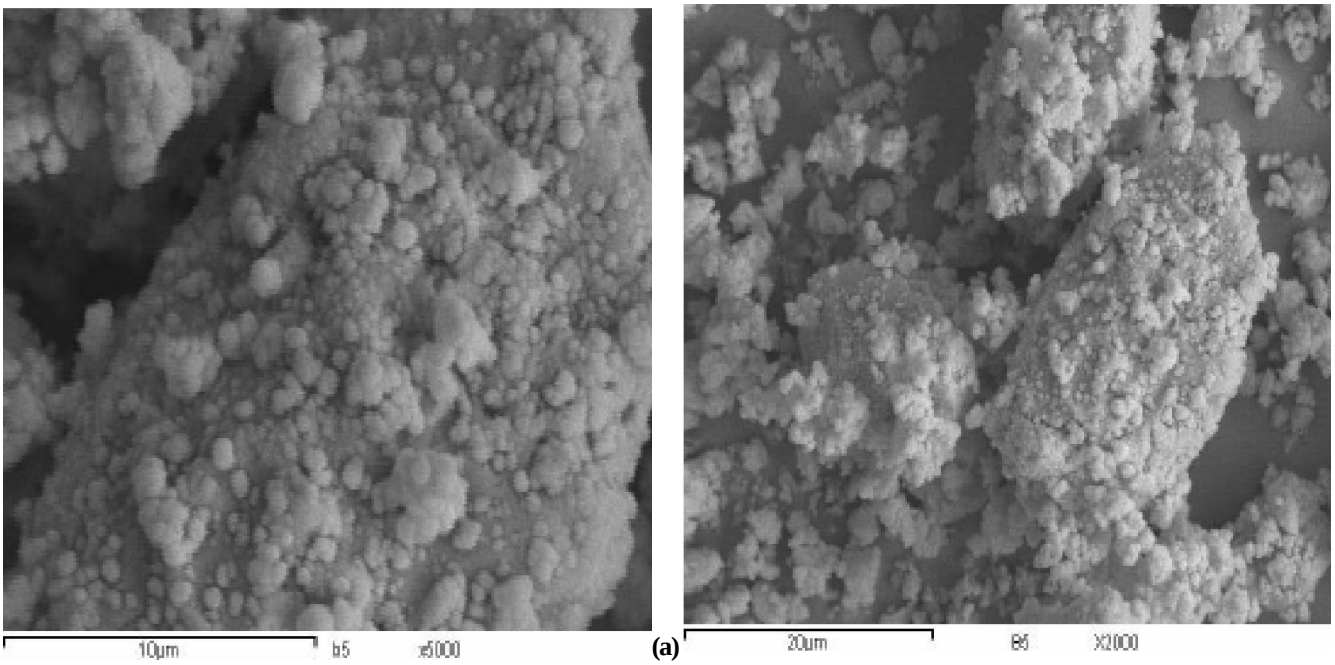

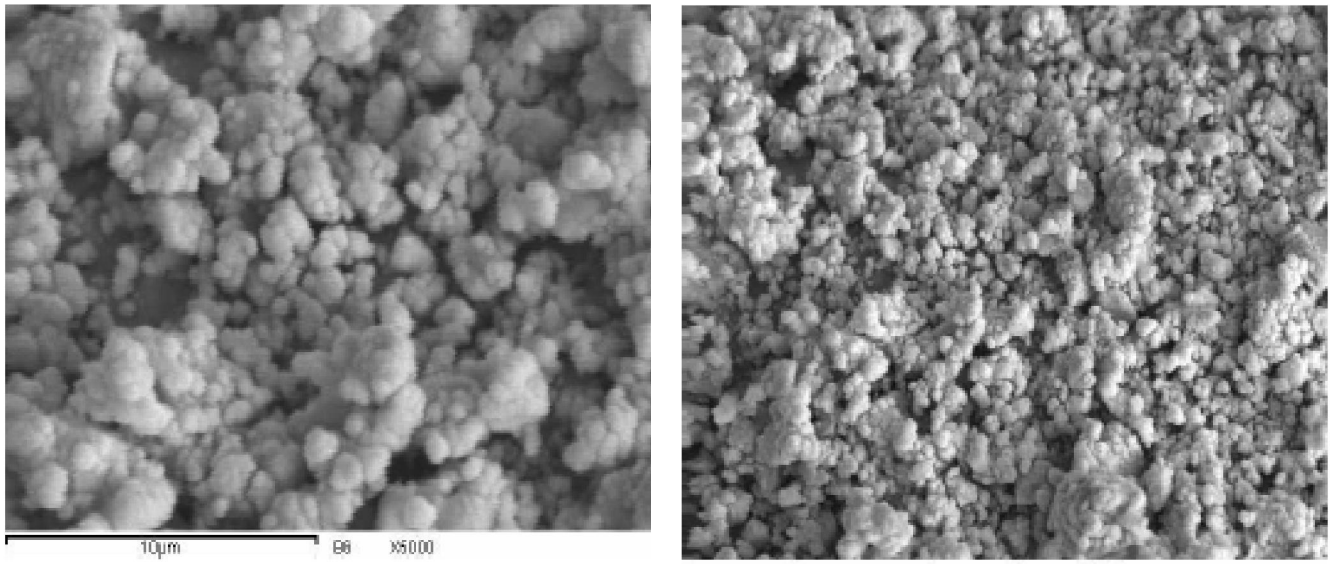


(e)

**Figure ($3_{a,c,e}$): SE-micrograph images recorded for pure and some selected Zr-doped 212-Bi-Sr-V-O system with two different magnification factors 2000x µm & 5000x µm: where (a): $Bi_2SrV_2O_9$, (c): $Bi_2SrV_{1.9}Zr_{0.1}O_9$ and (e): $Bi_2SrV_{1.7}Zr_{0.3}O_9$**

Sr-V-O regime. Furthermore, $ZrO_2$ does not detected in the grain boundaries which emphasis that Zr-ions substitute successfully on the crystal lattice on the vanadium sites.

## Thermal analyses measurements

Thermogravimetric analysis (TGA) and differential thermal analysis (DTA) were carried out in the temperature range from room temperature to 850°C at a heating rate of 10°C $min^{-1}$ on the green mixture of pure 212-BiSrVO and some selected Zr-doped samples with the general formula $Bi_2SrV_{2-x}Zr_xO_9$, where x=0.1, 0.3 mole.

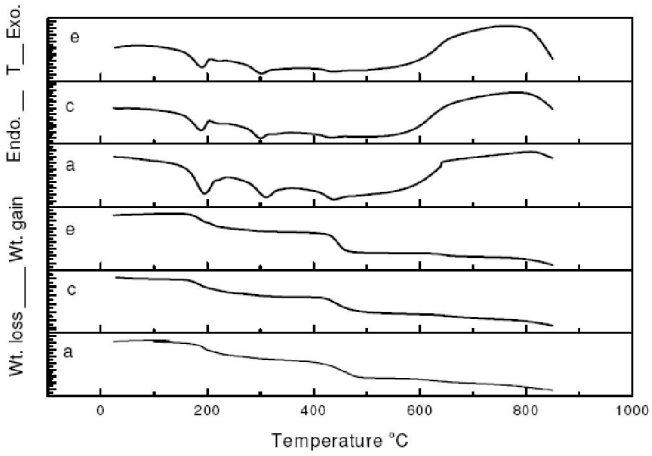


**Figure ($4_{a-c-e}$) : Thermo gravimetric (TGA) and differential thermal analyses(DTA) curves recorded for green mixture of pure and some selected Zr-doped 212-Bi-Sr-V-O system where (a): $Bi_2SrV_2O_9$, (c): $Bi_2SrV_{1.9}Zr_{0.1}O_9$ and (e): $Bi_2SrV_{1.7}Zr_{0.3}O_9$**

From TGA/DTA curves as shown in Figure ($4_{a-c-e}$), the TGA analysis can be divided into four steps, the first step occupies the region from room temperature till 230°C for which the weight loss occurred is attributed to the humidity and decomposition of $(NH_4)_2VO_3$ into $NH_3$ and vanadium oxide.

The second region from 230°C to 400°C at which $Bi_2(CO_3)_3$ is decomposed into $Bi_2O_3$ and $CO_2$. The third region of temperature from 400-660°C at which weight loss occurred is due to partial decomposition of $SrCO_3$ incorporated with high temperature solid state initial phase formation reaction. The fourth step occupying in the range 660-850°C is due to final decomposition of $SrCO_3$ and the final formation of solid state oxide[33-35]. The endothermic peaks above 400°C in DTA curves correspond to solid state reaction formation[33].

## Electron paramagnetic resonance measurements

Figure ($5_{a,c,e}$) explain the electron spin resonance (ESR) signals recorded for pure $Bi^{212}$ and some selected Zr doped samples with x=0.1, 0.3 mole.

It was shown that the effective g-values ($g_{iso}$) exhibit an increase from x=0.0 mole to x=0.3 mol due to strong coupling between $Zr^{4+}$ ion that substitutes $V^{5+}$ ion successfully at low dopant concentration Figure (6). These results of ESR proved that the anisotropy occurred as a result of Zr doping where $g_{eff}$ varies as function of x value[36-37].

Full Paper

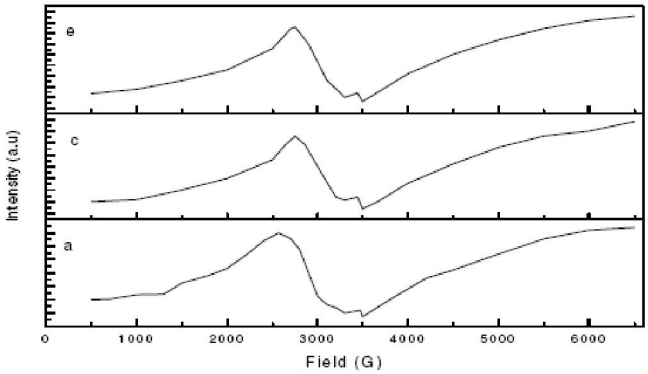


**Figure ($5_{a,c,e}$) : ESR spectra at room temperature for pure and some selected Zr-doped 212-Bi-Sr-V-O system where (a): $Bi_2SrV_2O_9$, (c): $Bi_2SrV_{1.9}Zr_{0.1}O_9$ and (e): $Bi_2SrV_{1.7}Zr_{0.3}O_9$**

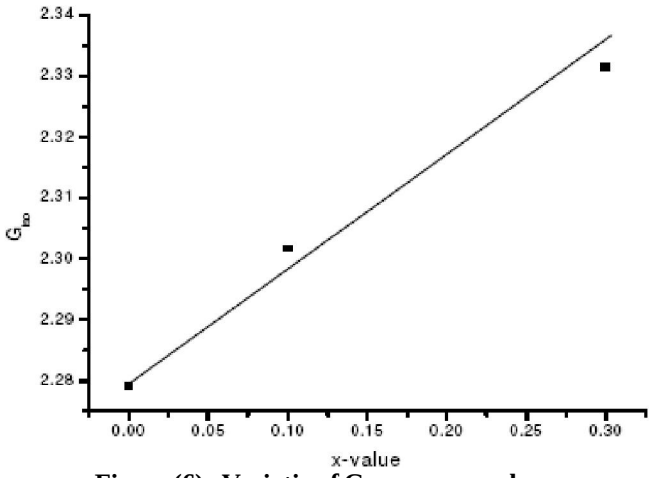


**Figure (6) : Variatio of $G_{iso}$ versus x-values**

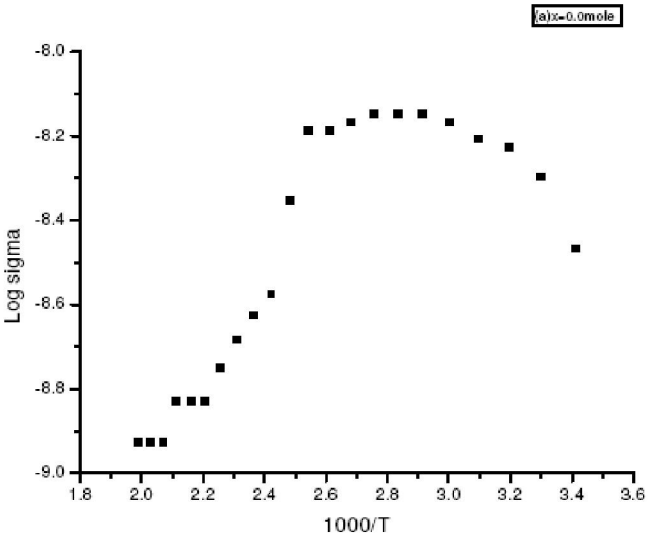


**Figure ($7_a$) : Variation of DC-electrical conductivity as a function of temperature for pure 212-Bi-Sr-V-O system**

## DC-Electrical conductivity measurements

Figure ($7_{a-f}$) displays the variation of DC-electrical conductivity as a function of reciprocal of absolute temperature for various $Zr^{4+}$ dopings. The data from Figure ($7_{a-f}$) exhibit conducting and semiconductor behavior since the conductivity increases as the temperature rise in case of conductor and the conductivity decrease as the temperature rise in case of semiconductor[38].

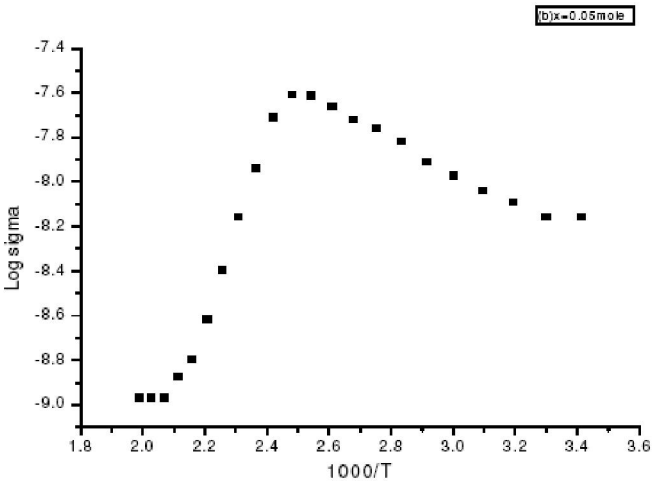


**Figure ($7_b$) : Variation of DC-electrical conductivity as a function of temperature for (b) $Bi_2SrV_{1.95}Zr_{0.05}O_9$**

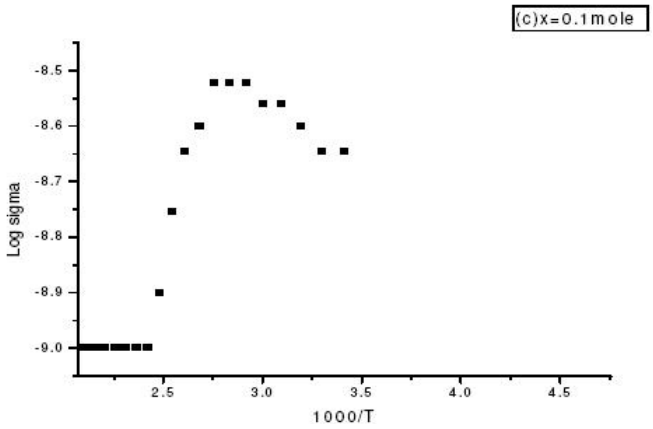


**Figure ($7_c$) : Variation of DC-electrical conductivity as a function of temperature for (c) $Bi_2SrV_{1.9}Zr_{0.1}O_9$**

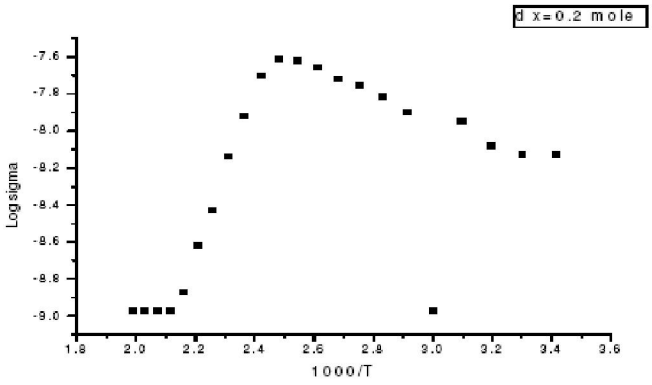


**Figure ($7_d$) : Variation of DC-electrical conductivity as a function of temperature for (d) $Bi_2SrV_{1.8}Zr_{0.2}O_9$**

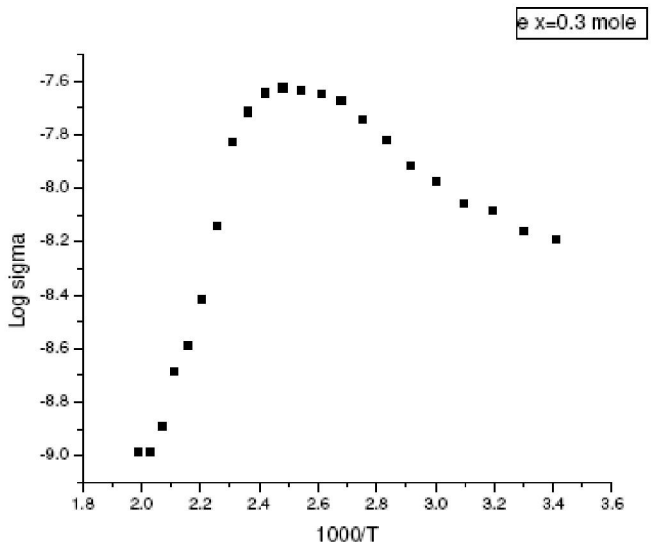


**Figure ($7_e$) : Variation of DC-electrical conductivity as a function of temperature for (e) $Bi_2SrV_{1.7}Zr_{0.3}O_9$**

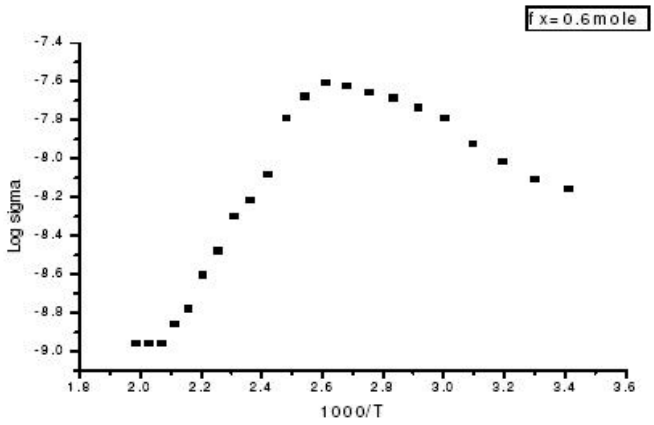


**Figure ($7_f$) : the variation of DC-electrical conductivity as a function of temperature for (f) $Bi_2SrV_{1.6}Zr_{0.4}O_9$**

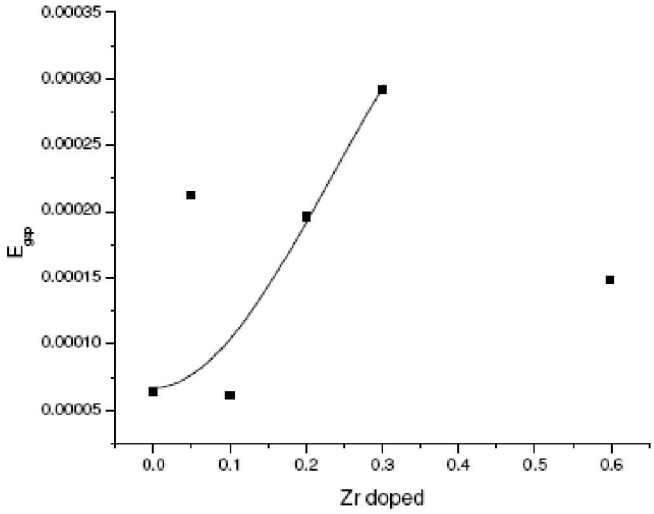


**Figure ($8_a$) : Variation of $E_{gab}$ versus Zr-content**

Figure ($8_{a,b}$) show the relation between the energy gap ($E_g$), number of $e^-$ in conduction band ($N_{cb}$) for Zr doped in which the $E_g$ and $N_{cb}$ increase as the ratio of Zr doping increases from x = 0.05 till x = 0.6 high concentration.

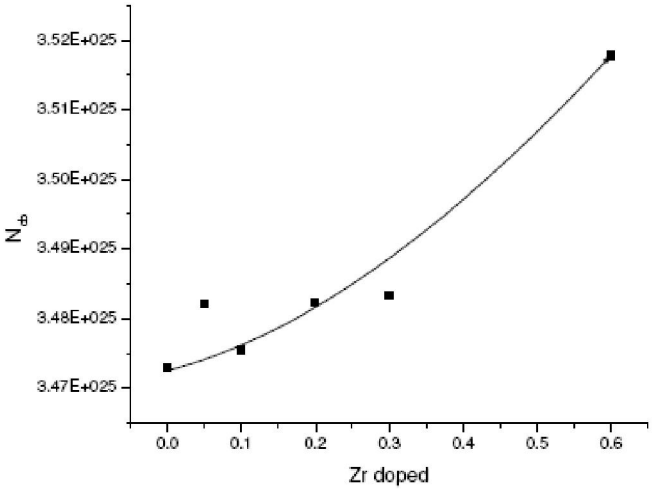


**Figure ($8_b$) : Variation of $N_{cb}$ versus Zr-content**

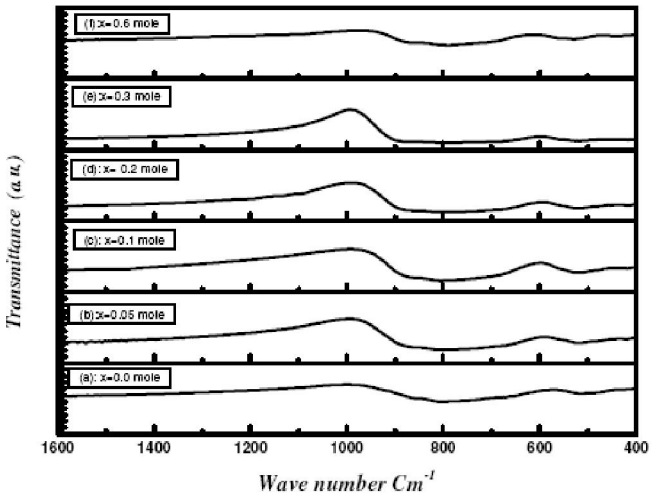


**Figure (9) : The room temperature solid infrared absorption spectra recorded for (a): Pure $Bi_2SrV_2O_9$, (b): $Bi_2SrV_{1.95}Zr_{0.05}O_9$,(c): $Bi_2SrV_{1.9}Zr_{0.1}O_9$, (d):$Bi_2SrV_{1.8}Zr_{0.2}O_9$, (e):$Bi_2SrV_{1.7}Zr_{0.3}O_9$, (f):$Bi_2SrV_{1.4}Zr_{0.6}O_9$**

$$\rho=\rho_o\, e^{-\Delta Eg / KT} \quad (1)$$

$$N_{cb}=AT^{3/2}\, e^{-Eg / 2KT} \quad (2)$$

## Solid infrared absorption spectral measurements

The infrared absorption spectra of pure $Bi_2SrV_2O_9$ and their Zr doped in the range of 500-2500$cm^{-1}$ are shown in Figure (9).

It is well Known that 212-Bi-Sr-V-$O_9\pm6$ system is mainly belongs to deficient perovskite structure and extra oxygen atom ) $O_9\pm6$). Oxygen nine converts it to distorted perovskite structure and consequently the com-

mon vibrational modes of IR-spectra of perovskite are clearly appear.

From Figure (9) we can summarize the different vibrational modes and their reasons as follows;

(a) The range from 400-600cm$^{-1}$ includes the most of infrared active phonons involving stretching modes of vibrating Bi-O, Sr-O and V-O/Zr-O plus bending modes of Bi-O-V, Bi-O-Sr, respectively.

(b) The Broad band around 800cm$^{-1}$ is mainly due to an increase in the free carrier scattering as reported in[39-40].

(c) The vibrational modes at ≈700-800cm$^{-1}$ is due to the effect of charge exchangrment of $V^{+5}/Zr^{+4}$ carriers which is enhanced by increasing Zr-dopings.

## CONCLUSION

In summary, 212-BiSrVO ceramics with various x-values were prepared by the solid state reaction method. X-ray diffraction proved that the compounds have distorted perovskite structure with hexagonal crystal form and the Zr substitution are successfully even at high concentration x=0.6 mole. The ferroelectric properties of the layered perovskite have been significantly enhanced with Zr doping. The DC-electrical show conducting and semiconducting behavior. The IR spectra displays that the system is belongs to deficient perovskite structure and extra oxygen atom) $O_9 \pm 6$).

## REFERENCES


[1] C.A.P.de Araujo, J.D.Cuchiaro, L.D.McMillan, M.C.Scott, J.F.Scott; Nature (London), **374**, 627-29 **(1995)**.

[2] J.F.Scott, C.A.P.de Araujo; Science, **246**, 1400-1405 **(1989)**.

[3] G.Z.Cao; in 'Advances in Materials Science and Applications'. Edited by D.L.Shi; Tsinghua University Press and Springer-Verlag, Beijing, China, 86-112 **(2001)**.

[4] J.F.Scott; in 'Thin Film Ferroelectric Materials and Devices'. Edited by R.Ramesh Kluwer, Norwell, MA, 115 **(1997)**.

[5] J.F.Scott; Ann.Rev.Mater.Sci., **28**, 79-100 **(1998)**.

[6] P.Duran-Martin, A.Castro, P.Millan, B.Jimenez; J.Mater.Res., **13**, 2565 **(1998)**.

[7] Y.Torii, K.Tato, A.Tsuzuki, H.J.Hwang, S.K.Dey; J.Mater.Sci.Lett., **17**, 827 **(1998)**.

[8] H.Watanabe, T.Mihara, H.Yoshimori, C.A.P.Araujo; Jpn.J.Appl.Phys., **34**, 5240 **(1995)**.

[9] J.shimoyama, J.Kasa, T.Morimoto, J.Mizusaki, H.Tagawa; Physica C, **931**, 185-189 **(1981)**.

[10] E.Diaz-Valdes, G.Pacheco-Malagon, G.Contreras-Puente, C.Mejia-Garcia, G.Andrade-Garay, J.Ortiz-Lopez, A.Conde-Gallardo, C.Falcony; Mater.Chem. Phys., **36**, 64 **(1993)**.

[11] K.C.Hewitt, X.K.Chen, X.Meng-Burany, A.E.Curzon, J.C.Irwin; Physica C, **251**, 192 **(1995)**.

[12] B.Aurivillius; Arkiv For Kemi, **1(58)**, 499-512 **(1949)**.

[13] B.Aurivillius; Arkiv For Kemi, **1(54)**, 463-80 **(1949)**.

[14] B.Aurivillius; Arkiv For Kemi, **2(37)**, 519 **(1950)**.

[15] T.Rentschler; Materials Research Bulletin, **32(3)**, 351-69 **(1997)**.

[16] T.Motohashi, Y.Nakayama, T.Ujita, K.Kitazawa, J.Shimoyama, K.Kishio; Phys.Rev.B, **59**, 1408 **(1999)**.

[17] J.Shimoyama, Y.Nakayama, K.Kitazawa, K.Kishio, Z.Hirio, I.Chong, M.Takano; Physica C, **281**, 69 **(1997)**.

[18] W.D.Wu, A.Keren, L.P.Le, B.J.Sternlieb, G.M.Luke, Y.J.Uemura; Phys.Rev.B, **47**, 8127 **(1993)**.

[19] Q.Z.Ma, G.H.Ca, Y.Li, N.Chen; China J.Low. Temp.Phys., **18**, 246 **(1996)**.

[20] Q.Z.Ma, X.Q.Huang, X.T.Xiong, Y.Li, G.H.Cao, T.B.Zhang; China J.Low Temp.Phys., **19**, 128 **(1997)**.

[21] V.Shrivastava, A.K.Jha, R.G.Mmendiratta; Physica B, **371**, 337 **(2001)**.

[22] R.R.Das, P.Bhattacharya, W.Perez, R.S.Katiyar; Ceram.Int., **30**, 1175 **(2004)**.

[23] C.A.P.de Araujo, L.D.Mc Millan, J.D.Cuchiaro, M.C.Scott, J.F.Scott; Nature (London), **374(6523)**, 627-629 **(1995)**.

[24] J.F.Scott, C.A.P.de Araujo; Ferroelectric memories, Science, **246(4936)**, 1400-1405 **(1989)**.

[25] B.Aurivillius; Ark.Kemi., **5**, 39-47 **(1952)**.

[26] E.C.Subbarao; Phys.Rev., **122(3)**, 804-807 **(1961)**.

[27] I.Coondo, A.K.Jha; Solid state Communications, **142**, 561-565 **(2007)**.

[28] J.Qiu, G.Z.Liu, M.He, H.S.Gu, T.S.Zhou, Physica B, **400**, 134-136 **(2007)**.

[29] I.coondoo, A.K.Sha, S.K.Aggawal, N.C.Soni; J.Electroceram., **16**, 393 **(2006)**.

**[30]** Y.Wu, G.Cao; J.Mat.Res., 15 **(2000)**.
**[31]** N.A.Hamed, R.ABD-Shukor; J.Materials Science, **35**, 2325-229 **(2000)**.
**[32]** M.Mimouni, M.F.Mosbah, A.Aminea, F.Kezzoula, A.Haouam, A.Boubellou; Physica B, **321**, 287-291 **(2002)**.
**[33]** M.A.Sekkina, K.M.Elsabawy; Physica C, **377**, 254-259 **(2002)**.
**[34]** Y.Srinivasa Rao, C.S.Sunandana; J.Materials Science Letters, 11 **(1992)**.
**[35]** R.H.Tahar, N.H Tahar, A.B.Salah; J.Crystal Growth, 307 **(2007)**.
**[36]** I.Onyszkieuicz, P.Czarnecki, R.Mienas, S.Robaszkiewiez, Physica B, C, **147(2-3)**, 166 **(1979)**.
**[37]** T.Hidaka; Phys.Rev.B, **20**, 2769 **(1979)**.
**[38]** A.Simpson, E.Robert; 'Introductory Electronics for Scientists & Engineers', 2nd Edition, Allyn and Bacon, **(1987)**.
**[39]** A.Memon, M.Khan, S.Adallal; Physica C, **9**, 235-240 **(1994)**.
**[40]** P.Qurong, X.Gao Jie, Z.Zengming, D.Zejum; Physica C, **70**, 269-274 **(2002)**.